ELSEVIER

Contents lists available at ScienceDirect

Environmental Pollution

journal homepage: www.elsevier.com/locate/envpol



Activation of percarbonate by water treatment sludge—derived biochar for the remediation of PAH-contaminated sediments*



Chang-Mao Hung ^a, Chin-Pao Huang ^b, Chiu-Wen Chen ^a, Chung-Hsin Wu ^c, Yi-Li Lin ^d, Cheng-Di Dong ^{a, *}

- ^a Department of Marine Environmental Engineering, National Kaohsiung University of Science and Technology, Kaohsiung City, Taiwan
- ^b Department of Civil and Environmental Engineering, University of Delaware, Newark, USA
- ^c Department of Chemical and Materials Engineering, National Kaohsiung University of Science and Technology, Kaohsiung City, Taiwan
- d Department of Safety, Health and Environmental Engineering, National Kaohsiung University of Science and Technology, Kaohsiung City, Taiwan

ARTICLE INFO

Article history:
Received 22 April 2020
Received in revised form
21 May 2020
Accepted 29 May 2020
Available online 27 June 2020

Keywords: Biochar Percarbonate Polycyclic aromatic hydrocarbon (PAH) Pyrolysis Sludge

ABSTRACT

Sludge from a groundwater treatment plant was used to prepare biochar by pyrolysis. The Fe–Mn rich biochar was used to activate percarbonate for the remediation of polycyclic aromatic hydrocarbons (PAHs) contaminated aquatic sediments. Results showed that the sludge–derived biochar (SBC) produced at a pyrolysis temperature of 700 °C was the most effective in activating percarbonate, which exhibited significant oxidative removal of PAHs. PAHs degradation took place via a Fenton-like oxidation manners, contributed from the Fe^{3+}/Fe^{2+} and Mn^{3+}/Mn^{2+} redox pairs, and achieved the highest degradation efficiency of 87% at pH₀ 6.0. Reactions between oxygenated functional groups of biochar and H_2O_2 generated of $O_2^{\bullet-}$ and HO_{\bullet} radicals in abundance under neutral and alkaline pH was responsible for the catalytic degradation of PAHs. Our results provided new insights into the environmental applications of SBC for the green sustainable remediation of organics-contaminated sediments and aided in reduction of associated environmental and health risk.

© 2020 Elsevier Ltd. All rights reserved.

1. Introduction

Aquatic sediment is a major sink for hazardous chemicals, which has become one of the most critical environmental issues worldwide (Zheng et al., 2019). For example, the rapid industrialization and growing scale of anthropogenic activities have increased discharge of persistent organic pollutants such as polycyclic aromatic hydrocarbons (PAHs), which, in view of their hydrophobicity and low water solubility, readily accumulate in aquatic sediments and pose significant threats to aquatic organisms and humans (Maletić et al., 2019). The US EPA has listed PAHs as priority control pollutants, as these carcinogenic, mutagenic, and teratogenic species with high bioaccumulation ability may adversely affect human health (Du and Jing, 2018). Therefore, much attention has been directed at the remediation and management of PAH-contaminated sediments (Meng et al., 2019; Han et al., 2019).

Sustainable approaches to the remediation of contaminated

* Corresponding author.

E-mail address: cddong@nkust.edu.tw (C.-D. Dong).

marine sediments remain highly sought after (Dong et al., 2017, 2018a,b; 2019a-c; 2020a,b). Among these approaches, advanced oxidation technologies (AOTs) such as Fenton oxidation allow one to efficiently degrade and mineralize contaminants in groundwater and soils but commonly require the use of liquid H₂O₂ (Fu et al., 2016). Recently, in situ oxidation relying on the production of hydroxyl radicals (HO \bullet /H₂O, E⁰ = 2.76 V vs. NHE) from solidsupported H₂O₂, e.g., sodium percarbonate (SPC) has received much attention. Compared to conventional Fenton reagents, AOT systems with solid-supported H₂O₂ feature the advantages of high stability, operation in a wide pH range, ease of handling, transportation safety, and high treatment efficiency (Danish et al., 2017). In these systems, non-selective HO• radicals are produced through heterogeneous electron transfer and therefore feature a significantly prolonged lifetime (Fu et al., 2017). Moreover, numerous agents such as non-metallic materials and transition metals can be used to activate SPC for HO• and O2• production (De Luna et al., 2020; Hung et al., 2020). Miao et al. (2015) reported that highperformance chelating agents such as citric acid monohydrate, oxalic acid, and glutamic acid improve the efficiency of tetrachloroethene degradation by increasing the concentration of Fe³⁺

^{*} This paper has been recommended for acceptance by Su Shiung Lam.

in solution, which leads to the continuous generation of reactive species such as HO• and O_2^{\bullet} , a typical Fenton process. Li et al. (2019a) studied the removal of PAHs from water using Fe–Mn binary oxide–modified biochar (Fe–Mn–BC) and achieved a significant reduction of naphthalene content in contaminated soils using photo–Fe–Mn–BC/H₂O₂ system. Danish et al. (2017) activated SPC by a zeolite-supported nanocopper bimetallic composite to remove trichloroethene from water and achieved a removal efficiency of >95%. The enhanced catalytic reactivity was ascribed to the presence of Fe³⁺/Fe²⁺ and Cu²⁺/Cu⁺ redox couples. Fu et al. (2017) studied the removal of benzene by an Fe(III)-activated SPC system and identified HO• and O₂• as the major species responsible for complete benzene degradation. Lemaire et al. (2013) investigated the remediation of PAH-contaminated soils by SPC and reported that the presence of Fe salts increased the degradation capacity of PAHs

Carbon-based materials such as biochar exhibits enhanced catalytic activity and are widely available, cheap, and environmental friendly (Wang et al., 2019a, b). In addition, biochar is chemically stable under both acidic and alkaline conditions and can be prepared from biowaste such as water treatment plant derived-sludge, which allows one to drastically reduce material cost. Raw biomaterials such as sludge have received much attention, because of their intrinsic floc structure and high organic carbon content, which enables the production of biochar that is rich in pore structure, large specific surface area, and abundant oxygenated functional groups with high metal affinity (Liu et al., 2019; Tao et al., 2019). The chemical structure and microporosity of biochar is known to strongly influence the sorption/desorption and chemical degradation of PAHs (Kołtowski et al., 2017). Moreover, magnetic biochar has been proposed as an ideal heterogeneous catalyst because of its high biocompatibility and ease of separation (Dong et al., 2019d, 2020b). Hung et al. (2016a,b) studied the Fe₃O₄-promoted decontamination of dye-polluted wastewater and reported high degradation capacity. Zhao et al. (2013) reported that the activation of persulfate (PS) at 60 °C, completely removed PAHs from soils and attributed the high PAH removal capacity to the generation of OH• and SO₄•. Recently, Dong et al. (2017) synthesized magnetic iron oxide-carbon composites for the removal of hazardous chemicals and reported effective catalytic degradation of PAHs in contaminated sediments. Thus, high catalytic efficiency is one of the main criteria of heterogeneous catalyst development.

Groundwater is an important source of drinking water in Taiwan because of the short supply of surface water (Kan et al., 2017). However, high Fe and Mn content in the Taiwanese groundwater has complicated the water treatment operation and produced large amounts of sludge, which becomes a significant engineering and environmental burden (Kan et al., 2012). Hence, much attention has been drawn to the pyrolysis of sludge to synthesize sludge-derived biochar (SBC), which features the advantages of high catalytic activity, thermal stability, and environmental friendliness, and is therefore a promising material for AOT applications (Zhang et al., 2015; Huang et al., 2020). However, the effect of pyrolysis temperature on the performance of SBC in the SPC-mediated oxidation of PAHs has not been investigated. The current study was based on the hypothesis that the SBC has the potential to contribute to enhance environmental sustainability, which was significant to understanding the SPC activation mechanism for the degradation of PAHs in sediments. Therefore, this work aimed to develop Fe-Mn-SBC for the remediation of PAH-contaminated marine sediments and evaluate the effect of SBC preparation temperature on the efficiency of SPC activation for the degradation of PAHs in sediments. Moreover, mechanistic insights into PAH degradation in the above system were gained using X-ray diffraction (XRD), Fourier transform infrared (FTIR) spectroscopy, UV-Vis spectroscopy, and X-ray photoelectron spectroscopy (XPS).

2. Experimental

2.1. Chemicals

 $2Na_2CO_3 \bullet 3H_2O_2$ (SPC; 20-30 wt% H_2O_2) was received from Sigma-Aldrich Co. Ltd. (St. Louis, USA). Acetone, methanol, and n-hexane (99.8%, HPLC grade) were purchased from Merck (Darmstadt, Germany). A standard solution containing 16 PAHs (at 80 ppm), standard internal deuterated PAH solution (4000 ppm), and standard surrogate solutions (2000 ppm) were purchased from AccuStandard Chem. Co. (New Haven, CT, USA). All chemicals were of analytical grade and used without further purification. Solutions for all experiments were prepared with DI water.

2.2. Sediment collection

Aquatic sediments (the top 0–15 cm) from the Kaohsiung Harbor (22°32.416′ N 120°20.639′E) in Southern Taiwan were scooped into glass bottles pre-washed with *n*-hexane. The bottles were immediately capped and kept frozen during transport to the laboratory. The samples were air-dried at 25 °C for 7 d, then homogenized, pulverized, and sieved through a 2-mm standard sieve. Subsequently, samples passing through a 0.5-mm sieve were homogenized using a mortar and freeze-dried for 72 h. The sediment composition was determined as loamy (34, 61, and 5 wt% sand, silt, and clay, respectively).

2.3. Preparation of biochar from groundwater treatment plant sludge

Dewatered sludge, collected from the Changhua Water Treatment Plant in central Taiwan, was used as the substrate in this study. The groundwater was a potable water source of the water purification plant at a treatment capacity of 30,000 m³/d. Specifically, the raw water, drawn from 12 deep wells, having Fe and Mn levels of 0.2-0.6 mg/L, was sequentially subjected to aeration, chlorination with sodium hypochlorite, and manganese green sand filtration (Kan et al., 2012). The content of Fe and Mn in the sludge were ~240,000 and 286 mg/kg, respectively. Raw sludge was airdried to constant weight (105 °C for 48 h) and sieved to remove particles larger than 150 µm. The water treatment plant derived-sludge biochar was prepared without any pretreatment using a one-step process of pyrolysis in a laboratory-scale furnace (NBD-01200, Nobody Materials Science and Technology Co., Ltd., Henan, China) at 300, 500, 700, or 900 °C, respectively, at a heating rate of 10 °C/min in purified N₂ (99.99%, 100 mL/min) flow. Biochar samples were labeled as SBCX, where X being the pyrolysis temperature.

2.4. PAH degradation experiments

PAH degradation tests were carried out in borosilicate glass bottles (40 mL volume) containing 1 g of sediment and 25 mL of SPC solution (PAH:SPC molar ratio = 1:1 to 1:100). SBC (0.83–6.67 g/L) was then added into the solution. The sample vials were manually shaken for ~30 s and further shaken in a constant-temperature (25 °C) water bath shaker (SB-9D, Hipoint Corporation, Kaohsiung, Taiwan) at 200 rpm for 6 h. All experimental and control runs were triplicated. At predetermined reaction time, SPC-mediated PAH degradation reaction was quenched with methanol. Then the mixture was sonicated after the addition of solvent (acetone:n-hexane, 1:1 v/v) to extract the liquid phase for the determination of residual PAHs. PAH concentration was determined by gas

chromatograph (Agilent Technologies, Model 6890, CA, USA) equipped with mass-selective detector (Agilent Technologies, Model 5975, CA, USA). The PAHs analyzed included: naphthalene (NA), acenaphthylene (ACY), acenaphthene (ACE), fluorene (FL), phenantrene (PH), anthracene (AN), fluoranthene (FLU), pyrene (PY), benzo[a]anthracene (BaA), chrysene (CH), benzo[b]fluoranthene (BbF), benzo[k]fluoranthene (BkF), benzo[a]pyrene (BaP), indeno[1,2,3-cd]pyrene (IP), dibenzo[a,h]anthracene (DA), and benzo[g,h,i]perylene (BP).

2.5. Characterization of prepared sludge biochar (SBC)

XRD analysis was conducted with Diano-8536 diffractometer using Cu K α radiation source. FTIR spectra were obtained with FT-700 spectrometer (Horiba, Japan) in 32 scans at spectral resolution of 4 cm $^{-1}$. UV–Vis spectra were acquired in the wavelength range of 200–800 nm under ambient conditions on a U-3900 spectrophotometer (Hitachi, Japan) equipped with an integration sphere (diffuse reflectance mode). XPS analysis (AXIS Ultra DLD, Kratos Analytical Ltd., Manchester, UK) gave the chemical state of major elements on SBC surface. Electron paramagnetic resonance spectroscopy (EPR; EMX-10/12, Bruker, Germany) with DMPO (0.1 M) as a spin-trapping agent was used to qualify and quantify the production O_2^{\bullet} and HO \bullet radicals, which concentration was determined, after correcting for background-noise intensity of DMPO- O_2^{\bullet} and DMPO-HO \bullet peaks, respectively.

2.6. PAH analyses

PAHs were analyzed with gas chromatography-mass spectrometry and Agilent split/splitless injector (Model 7683B, 1-min splitless time, 60-mL/min flow rate) in selected ion monitoring mode. The injector, transfer line, and ion source temperatures equaled 300, 280, and 230 °C, respectively. Separation of PAHs was carried out using capillary column (HP-5MS, Hewlett-Packard, Palo Alto, CA, USA), which length was 30 m, inner diameter was 0.25 mm, and film thickness was 0.25 μm . The carrier gas was Helium at a constant flow rate of 1 mL/min. The initial column temperature 40 °C was held for 1 min, raised to 120 °C at 25 °C/min, further increased to 160 °C at 10 °C/min, and finally increased to 300 °C at 5 °C/min. Satisfactory coefficients of determination ($r^2=0.98$) were obtained for each calibration curve.

3. Results and discussion

3.1. Characterization of SBC samples

XRD peaks at $2\theta = 30.1^{\circ}$, 35.5° , 43.2° , 53.6° , 57.0° , and 62.7° were ascribed to the (220), (311), (400), (422), (511), and (440) planes of Fe₃O₄, respectively (Fig. 1a) (Dong et al., 2019c). The peaks at

 $2\theta = 28.9^{\circ}$, 32.3°, 36.1°, 50.7°, and 59.8° were assigned to the (112), (103), (211), (105), and (224) facets of Mn₃O₄ (Li et al., 2016), respectively. As the pyrolysis temperature was increased from 700 to 900 °C, the peak intensity of (311) of Fe₃O₄ and (112) of Mn₃O₄ were significantly changed, likely due to increase in crystallinity and structural stability. Results indicated the presence of Fe₃O₄ induced the crystallization of Mn₃O₄ in SBC. Peaks at 26.2° and 43.9° were attributed to the (002) and (100) planes of amorphous graphite, respectively, indicating the presence of aromatic rings with increased π -polarity on the SBC surface, which enabled strong π -electron donor-acceptor interactions between SBC and aromatic compounds (Dong et al., 2018a). The sharpness of XRD peaks reflected the presence of highly crystalline Fe₃O₄ on the surface of SBC, which contributed to the magnetic property (Jung et al., 2016). Two sharp FTIR peaks at 480 and 577 cm⁻¹ represented the Fe-O stretching vibrations of Fe₃O₄ nanoparticles (Fig. 1b). The strong peak at ~1539 cm⁻¹ was attributed to carboxylate groups interacting with Fe₃O₄ particles, while peaks at 643 and 522 cm⁻¹ reflected Mn-O bond vibrations, and those at 1405 and 794 cm⁻¹ represented the vibration of Mn–O–Mn units (Kumar et al., 2016). SBC700 showed a broad band at \sim 3400 cm⁻¹, which reflected the presence of surface -OH groups. Moreover, signals at 1036, 1619 and 1558 cm $^{-1}$ corresponded to C-O-C, C=C, and C=0 bond stretching vibrations in the aromatic ring, respectively, while the strong band at 1640 cm^{-1} was ascribed to hydroxyl bending vibrations (Xu et al., 2012). The oxygen-containing functional groups (i.e., hydroxyl and carbonyl) present on the SBC surface were believed to act as electron donors and SPC activator, and also were considered as reactive sites for the adsorption and degradation of organic contaminants (Wang et al., 2020). The strong peak of C-O-C and C=C aliphatic/ether stretching on SBC700 indicated that aromatic carbon compounds played a central role on biochar structure (Wang et al., 2019a, b). However, the intensity of C=C and C=O groups on the SBC surface were weakened at 900 °C due to the decomposition of organic substances in the sludge during the pyrolysis process. Biochar prepared from organic residues tended to have abundant surface oxygenated functional groups, which greatly expanded its potential to environmental remediation application (Mohamed et al., 2015). Moreover, in certain geochemical environment such as pH, oxidation-reduction potential (ORP), and metal ion, biochar promoted generation of reactive oxygen species (ROSs) that efficiently enhanced the degradation of contaminants (Fang et al., 2015). A split of absorbance maxima of SBC700 was observed in the UV-Vis spectrum centered at 260 and 340 nm, corresponding to $O^{2-} \rightarrow Mn^{2+}$ and $O^{2-} \rightarrow Mn^{3+}$ charge transfer (Guo et al., 2018) (Fig. 1c).

3.2. PAHs degradation over SBC

The total sediment PAHs concentration was 1005 ± 9.4 mg/kg.

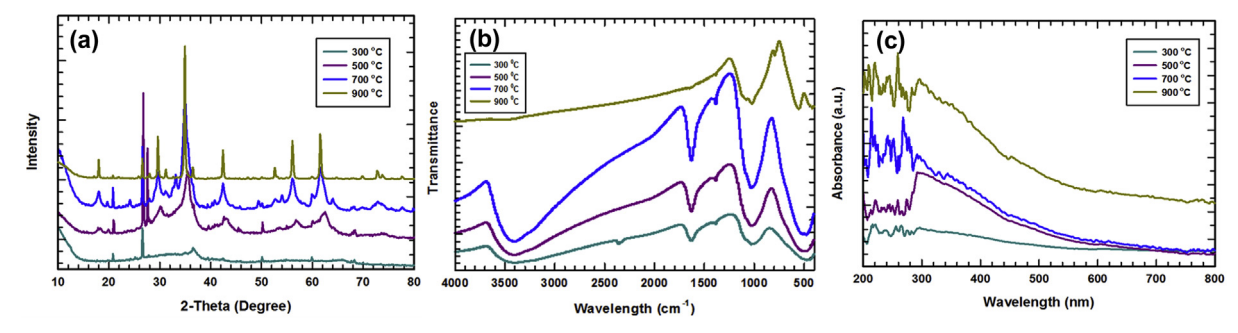


Fig. 1. The (a) XRD pattern, (b) FTIR and (c) UV—Vis spectra of SBC catalyst.

which was correspondent to medium to high contamination level according to Baumard et al. (1998). PH, FLU, and PY were the primary PAHs, with the four-ring PAHs (FLU, PY, BaA, and CH) being accounted for 58% of the total PAH content. The highest individual concentration was observed for PH (242 ± 9.8 mg/kg) and FLU $(208 \pm 16 \text{ mg/kg})$. The extent of PAH degradation was monitored for SPC dosages from 2 \times 10⁻⁵ to 2 \times 10⁻³ M (i.e., from a Σ [PAH] to [SPC] molar ratio of 1:1 to 1:100) (Fig. 2a), with the highest total PAH degradation efficiency of 44% occurred at SPC concentration of 2×10^{-4} M (or Σ [PAH] to [SPC] molar ratio of 1:10). Thus, SPC was efficient in degrading organic contaminants, consistent with results reported by Fu et al. (2016), who suggested that reactive •OH and O₂ radicals contribute to PAHs degradation at high SPC concentration. However, further increase in SPC dosage led to decrease in PAHs degradation efficiency due to the consumption or scavenging of •OH radicals by excess SPC (Lemaire et al., 2013). Furthermore, the efficiency of the removal of individual PAH was closely affected by molecular weight and number of ring. PAH is known to cover hundreds of individual congeners with two or more fused aromatic rings, which can be divided into those of low molecular weight (LMW) (two and three rings) and high molecular weight (HMW) (four to six rings). LMW PAHs are more responsive to oxidation than that of HMW because of greater water solubility (Mojiri et al., 2019). Herein, five PAHs (LMW PAHs: ACE, ACY, and NA; HMW PAHs: DA and IP) were detected in sediments at relatively low levels, and the highest degradation efficiency occurred on ACY (90%), NA (78%), and BP (76%) (Fig. 2b). The optimal SPC level for PAH degradation was 2×10^{-4} M, and the degradation efficiency 91, 61, and 54%, respectively, for the three-, four-, and five-ring HMW PAHs under otherwise identical experimental conditions (Fig. 2c). The kinetics of PAH oxidation over SBC was readily described by a pseudo-first-order model. The observed rate constant (k_{obs}) was determined from the slope of the linear plot of $ln(C/C_0)$ vs. time (t),

where C_0 and C are PAH concentration at times zero and t, respectively. As shown in Fig. 2d, the greatest $k_{\rm obs}$ (4.3 × 10⁻² h⁻¹) occurred at Σ [PAH]:[SPC] ratio of 1:100, exceeding that of 1:1 ($k_{\rm obs}$, 5.0 × 10⁻³ h⁻¹) almost by 8.6 folds. The presence of abundant HO• radicals contributed to the efficient PAHs degradation.

Pyrolysis temperature was found to greatly influence biochar properties (Chen et al., 2016). Fig. 3a shows the effect of pyrolysis temperature on the preparation of SBC and PAH degradation. Results demonstrated that SBC700 was most effective in SPC activation toward PAH degradation with 62%. Biochar has been reported to activate H₂O₂ via single electron transfer from persistent free radicals to H₂O₂ to produce •OH for organic contaminant degradation (Fang et al., 2014). Therefore, SBC catalyzed SPC activation and facilitated electron transfer among surface species. The SBC700/SPC system exhibited the highest degradation efficiency of 65, 56, and 65% for PH, PY, and FLU, respectively (Fig. 3b). The degradation efficiency of six-, five-, and four-ring PAHs was 87, 66, and 63%, respectively (Fig. 3c). The $k_{\rm obs}$ value was 1.4×10^{-2} , 6.6×10^{-2} , 11.8×10^{-2} , and 6.4×10^{-2} h⁻¹ for SBC300, SBC500, SBC700, and SBC900, respectively (Fig. 3d). Based on the above results, the SBC prepared at 700 °C was selected for further XPS analysis. Moreover, XPS peaks of SBC700 at 726.7 and 713.6 eV were assigned to the Fe2p_{1/2} and Fe2p_{3/2} transitions of Fe(II) and Fe(III), individually (Dong et al., 2019b) (Fig. 4a). The Mn $2p_{3/2}$ and Mn $2p_{1/2}$ 2 spectra could be deconvoluted into peaks at 642.6 and 654.7 eV, which confirmed the presence of Mn₃O₄ (Xia et al., 2019) (Fig. 4b). The strong C 1s peak at 285.8 eV indicated the presence of carboncontaining functional groups (Fig. 4c). Furthermore, active oxygen (O_{ads}) could be produced by O-O bond cleavage on the surface of Fe₃O₄ catalysts. It must be noted that Fe²⁺ and Mn²⁺, as electron donors, catalyzed the decomposition of SPC anions and thus enhanced PAH degradation. It has been reported that Fe²⁺ and Mn^{2+} can activate H_2O_2 to generate •OH and $O_2^{-\bullet}$, powerful

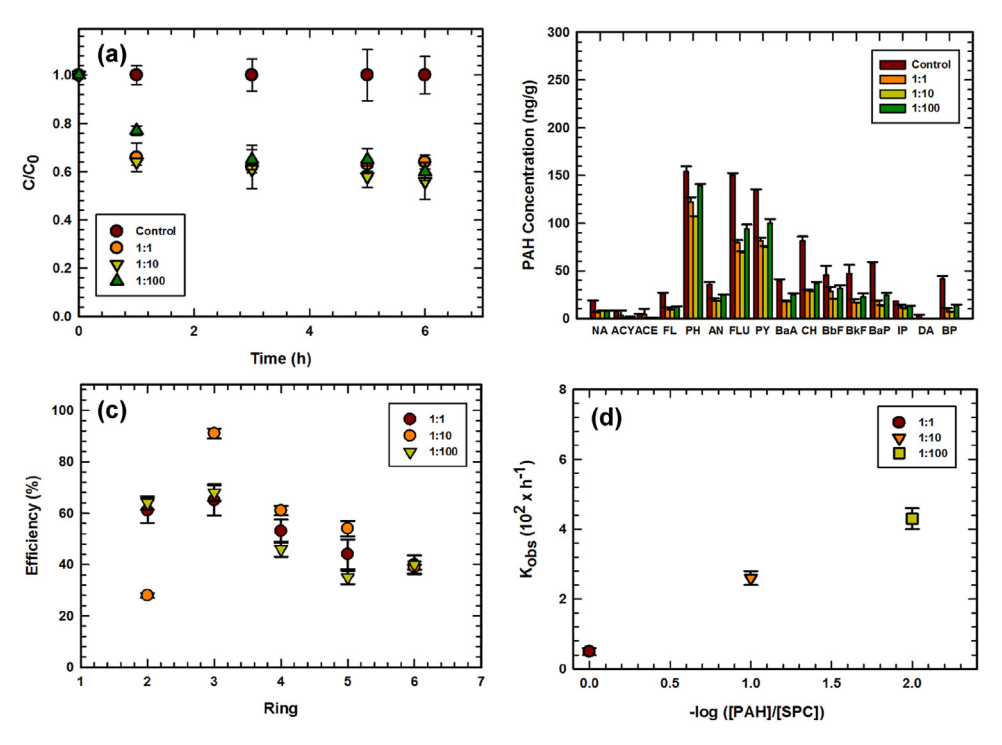


Fig. 2. The effect of sodium percarbonate (SPC) concentration on polycyclic aromatic hydrocarbon (PAH) degradation. (a) Change of different molar ratios of \sum PAH: SPC. (b) Distribution of PAH degradation products at t = 6 h. (c) Degradation efficiency of PAH as a function of ring numbers. (d) Rate constant of PAH degradation. Values are expressed as the mean \pm standard deviation of triplicate samples. Experimental conditions: sediment = 1.00 g, reaction volume = 40 mL, T = 25 °C, pH₀ = 9.0, molar ratios of \sum PAH: SPC = 1: $10^{\circ}-10^{2}$.

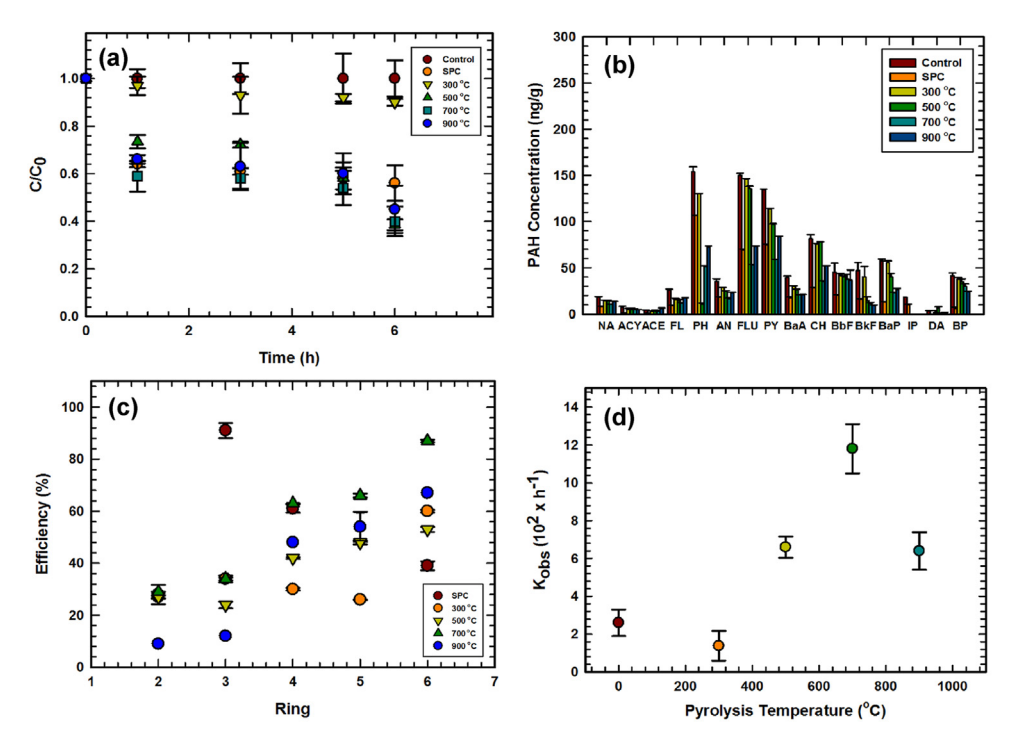


Fig. 3. The effect of pyrolysis temperature on polycyclic aromatic hydrocarbon (PAH) degradation. (a) Change of different pyrolysis temperature. (b) Distribution of PAH degradation products at t=6 h. (c) Degradation efficiency of PAH as a function of ring numbers. (d) Rate constant of PAH degradation. Values are expressed as the mean \pm standard deviation of triplicate samples. Experimental conditions: sediment = 1.00 g, reaction volume = 40 mL, T=25 °C, $PH_0=9.0$, $PH_0=9.0$

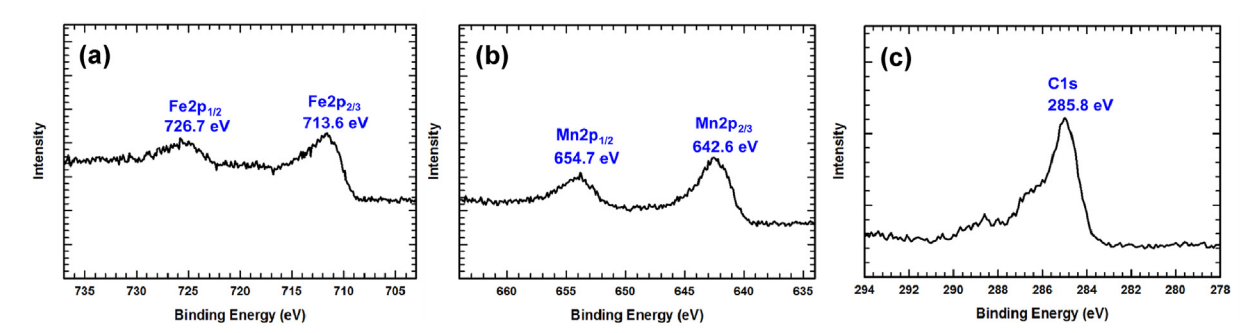


Fig. 4. X-ray photoelectron spectroscopy (XPS) spectrum of SBC catalyst. (a) Fe2p, (b) Mn2p and (c) C1s.

oxidants capable of effectively decomposing aqueous contaminants (Li et al. (2019a,b); Xia et al., 2019). Treatment of the PAHscontaminated sediments with SBC for 6 h results in the highest PAH removal efficiency, which demonstrated that SBC played a crucial role in controlling the catalysis capacity. SPC activation over SBC that generated •OH and O_2^{\bullet} through the Haber-Weiss mechanism was probably initiated by a special interphase surface that produced Fe^{2+} and Fe^{2+} and

Further experiments to explore the effect of SBC dosage on PAH degradation in the SBC/SPC system were conducted using SBC700 at different doses (0.83–6.67 g/L) and fixed SPC loading (2 \times 10⁻⁴ M). The extent of PAH removal was almost 85% at SBC dose of 1.67 g/L, whereas, the PAH degradation was 81% when the

SBC dose was 6.67 g/L in reaction time of 6 h (Fig. 5a). In general, the increase in catalyst dosage accelerated the decomposition of SPC to \bullet OH and O_2^{\bullet} because of abundant redox centers and sufficient active species serving as electron donors. However, the number of active sites on the reactants can be reduced due to agglomeration of catalyst particles at a high dosage (Mian and Liu, 2018). At the maximal SBC dose of 6.67 g/L, degradation efficiency of 84, 80, and 84% occurred for PH, PY, and FLU, respectively (Fig. 5b), while the degradation efficiency of the six-, five-, and four-ring PAHs was 97, 89, and 87%, respectively (Fig. 5c). The k_{obs} value at SBC dose of 0.83, 1.67, 3.33, and 6.67 g/L was 9.5×10^{-2} , 13.1×10^{-2} , 6.6×10^{-2} , and 9.5×10^{-2} h⁻¹, respectively (Fig. 5d). The ability of Fe²⁺ and Mn²⁺, when present in excess quantity, to scavenge \bullet OH radicals decreased the efficiency of PAH degradation (Ruan et al., 2019).

PAH degradation in the SBC/SPC system was evaluated at initial pH values of 3.0-11.0. Fig. 6a shows that substantial PAH degradation occurred at pH $_0$ 6.0 (87%) and 11.0 (85%) over 6 h, whereas a slightly decreased efficiency of 83% at pH $_0$ 3.0 was observed. The results demonstrated that PAH degradation by SBC–activated SPC

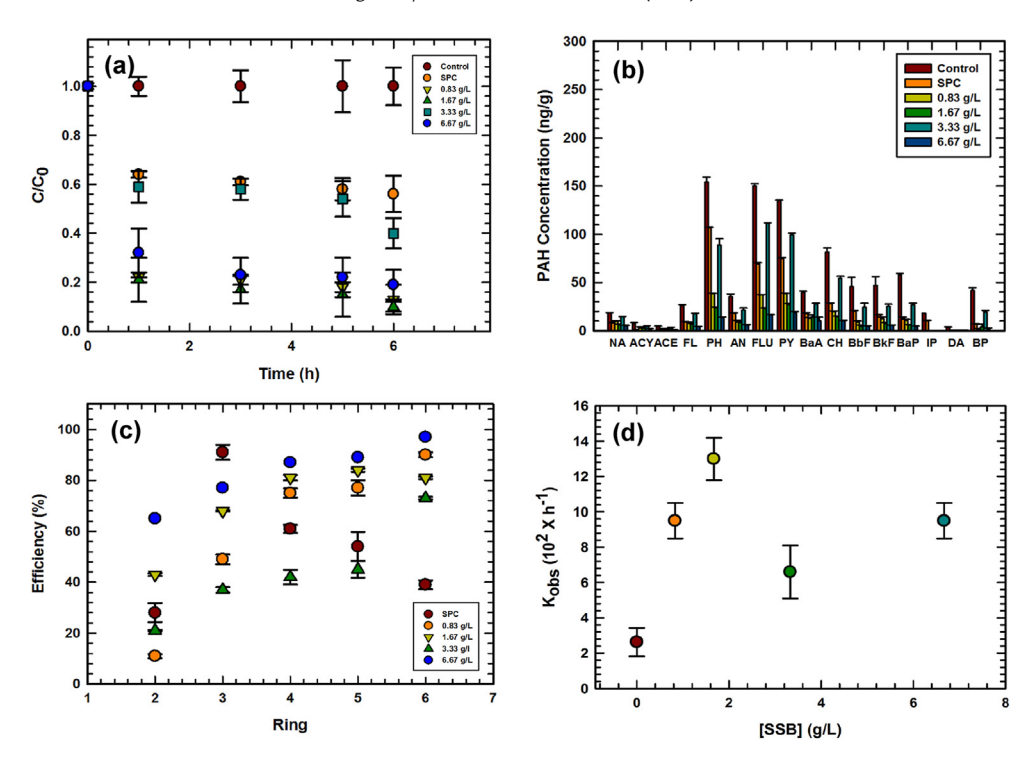


Fig. 5. The effect of SBC catalyst dosage on polycyclic aromatic hydrocarbon (PAH) degradation. (a) Change of different SBC dosage. (b) Distribution of PAH degradation products at t=6 h. (c) Degradation efficiency of PAH as a function of ring numbers. (d) Rate constant of PAH degradation. Values are expressed as the mean \pm standard deviation of triplicate samples. Experimental conditions: sediment = 1.00 g, reaction volume = 40 mL, T=25 °C, $PH_0=9.0$, $PH_0=9.0$

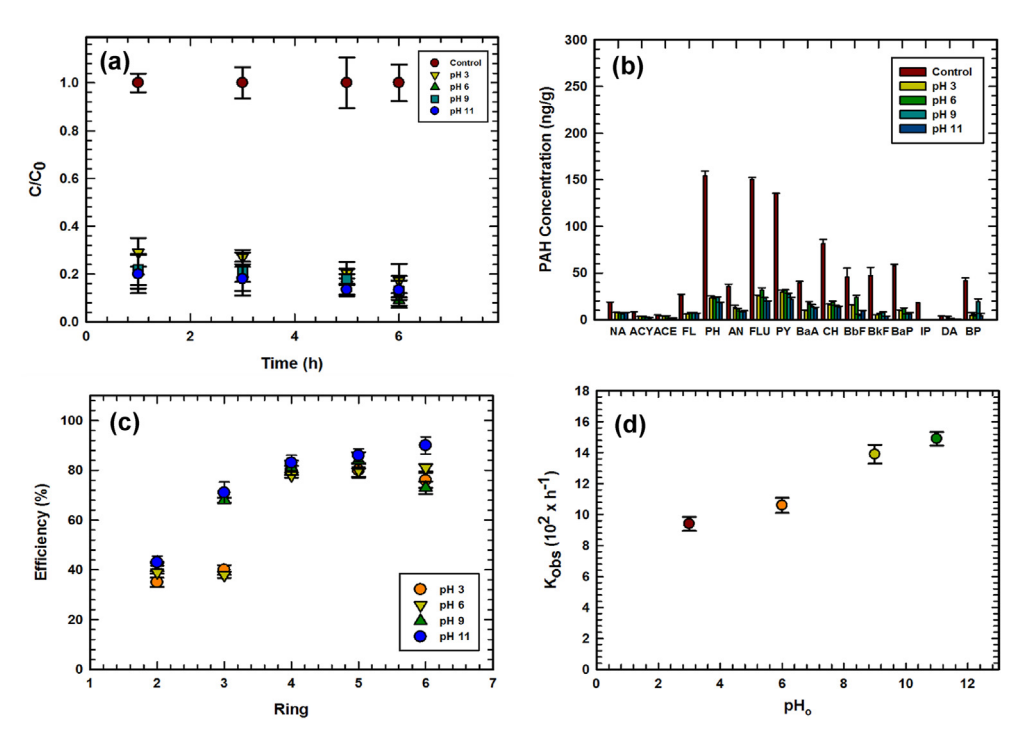


Fig. 6. The degradation of polycyclic aromatic hydrocarbon (PAH) as a function of initial pH in the presence of SBC catalyst. (a) Change of different initial pH. (b) Distribution of PAH degradation products at t=6 h. (c) Degradation efficiency of PAH as a function of ring numbers. (d) Rate constant of PAH reduction. Values are expressed as the mean \pm standard deviation of triplicate samples. Experimental conditions: sediment =1.00 g, reaction volume =40 mL, T=25 °C, [SBC] =1.67 g/L, [SPC] $=2\times10^{-4}$ M.

was favored under neutral and alkaline conditions, due to the weakly basic nature of SPC and its ability to slightly increase the pH of the sediment matrix. Under basic conditions, more \bullet OH radicals were produced through the reaction between SPC and H_2O/OH^- .

The sediment pH was well buffered by SPC, therefore, no apparent inhibition of PAH degradation occurred at pH₀ 11.0, i.e., the SB/SPC system could function in a wide pH range. CO₃[•] radicals have been reported to be more stable at near-neutral than at acidic pH (Cui

et al., 2017). The initial solution pH of the SBC/SPC system was 9.0. and hence, a significant amount of CO₃[•] was available. At the optimal pH (pH 6.0) for PAH degradation, the degradation efficiencies of PH, PY, and FLU equaled 85, 77, and 79%, respectively (Fig. 6b), while the corresponding numbers for six-, five-, and fourring PAHs equaled 90, 86, and 83%, respectively (Fig. 6c). The $k_{\rm obs}$ value was 10.7×10^{-2} , 14.0×10^{-2} , 9.5×10^{-2} , and 14.9×10^{-2} h at pH₀ 3.0, 6.0, 9.0, and 11.0, respectively (Fig. 6d), Overall, PAH degradation was favored by high pH. The fastest degradation at pH₀ 11.0 was ascribed to strong PAHs adsorption on SBC at alkaline pH (Li et al., 2019a,b). Thus, SBC-catalyzed PAHs oxidation by SPC was effective in the neutral to alkaline pH region (in which Fe and Mn precipitation was avoid) and was superior to conventional Fenton process. Furthermore, since •OH radical was stable in neutral aqueous media, pH would markedly affect SPC activity. The dissolution of Fe₃O₄ and Mn₂O₃ released Fe²⁺ and Mn²⁺, respectively, which tended to increase the degree of SPC activation and subsequent generation of •OH/O₂•. Excessive Fe²⁺ or Mn²⁺ enhanced the generation of •OH and accelerated electron transfer among surface species, thereby enhanced PAH degradation. In essence, biochar acted as an electron shuttle to mediate electron transfer reactions among chemical species involved in the Fenton-like system (Xia et al., 2019). Numeral mechanisms, including columbic forces, hydrogen bond, and Lewis acid-base complexation, were responsible for PAHs oxidation in the SBC/SPC system (Wang et al., 2019a, b). Consequently, control of the SBC dose could minimize the inhibitory effects of SBC on •OH/O2 production. Increasing pH decreased the oxidation capacity of •OH because of concomitant enhancement of •OH scavenging. Further, pH also affected the adsorption and catalytic capacity of biochar toward PAHs. The results indicated that PAHs removal by the SBC/SPC process was not significantly influenced by pH (Ahmad et al., 2014), rather efficient PAH degradation occurred over a wide pH range of 3.0-11.0.

Free radical generation due to SPC activation over SBC was probed by EPR (Fig. 7). Pure water in the presence of DMPO, i.e., exhibited no spins capture, while signal characteristic of 5,5-dimethylproline-(2)-oxyl-(1) (DMPOX) occurred when DMPO was added to the SPC solution. Two radical adducts were detected when SBC was present together with DMPO and SPC. Among the two signals, the dominant one was ascribed to DMPO-O $_2^{\bullet}$, indicating the generation of O $_2^{\bullet}$ and its participation in PAH degradation, while the weaker signal was assigned to DMPO-HO $_2^{\bullet}$, which was

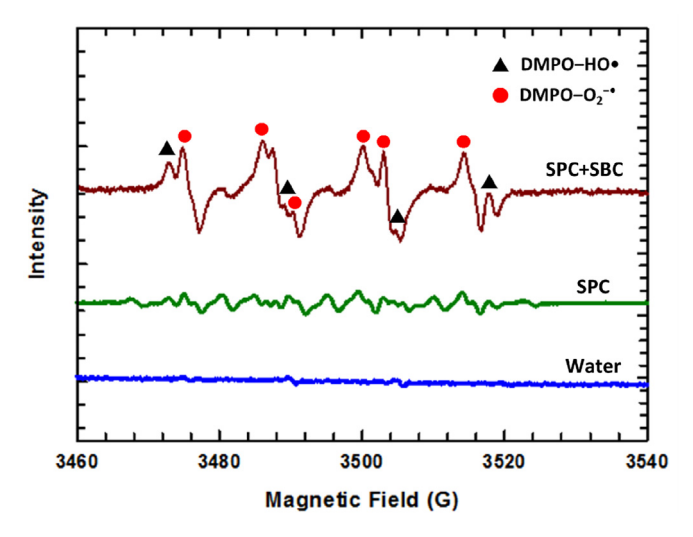


Fig. 7. Electron paramagnetic resonance (EPR) spectra of radical adducts trapped by 5,5-dimethyl-1-pyrroline N-oxide (DMPO) of the SBC catalyst.

evidenced of contribution of HO• to PAH degradation in complicated sediment matrix. The results demonstrated that SPC activation by SBC formed of a large amount of O_2^{\bullet} . Fe^{2+} created oxygen vacancies, adsorption sites for O_2 , that formed active chemisorbed oxygen on the SBC surface (Dong et al., 2019c). Further cleavage of O–O bonds on the SBC surface produced active oxygen (O_{ads}). The addition of SPC to water released H_2O_2 (Eq. (1)), which was further decomposed to $HO_2\bullet$, O_2^{\bullet} , and H^+ (Eqs. (2)–(5)) that triggered a series of synergistic reactions, such as electron transfer and formation of other radicals (Lin et al., 2017). The Fe^{2+} and $Factorize{Mn}^2$ and $Factorize{Mn}^2$ to form $Factorize{Mn}^2$ and $Factorize{Mn}^$

$$2Na_2CO_3 \cdot 3H_2O_2 \rightarrow 2Na_2CO_3 + 3H_2O_2$$
 (1)

$$2H_2O_2 \rightarrow 2H_2O + O_2$$
 (2)

$$H_2O_2 \rightarrow HO_2^{\bullet} + H^+ \tag{3}$$

$$HO_2^{\bullet} \rightarrow O_2^{-\bullet} + H^+ \tag{4}$$

$$O_2^{-\bullet} + 2H_2O \rightarrow H_2O_2 + O_2 + H^+$$
 (5)

$$Fe^{2+} + H_2O_2 \rightarrow Fe^{3+} + HO_{\bullet} + OH_{-}$$
 (6)

$$Fe^{3+} + H_2O_2 \rightarrow Fe^{2+} + HO_2 + H^+$$
 (7)

$$Fe^{3+} + H_2O_2 \rightarrow Fe^{2+} + O_2^{-\bullet} + 2H^+$$
 (8)

$$Fe^{3+} + O_2^{-\bullet} \rightarrow Fe^{2+} + O_2$$
 (9)

$$Fe^{3+} + HO_{2} \rightarrow Fe^{2+} + O_{2} + H^{+}$$
 (10)

$$Mn^{2+} + H_2O_2 \rightarrow Mn^{3+} + HO \bullet + OH^-$$
 (11)

$$Mn^{3+} + H_2O_2 \rightarrow Mn^{2+} + HO_2 \cdot + H^+$$
 (12)

$$Mn^{3+} + H_2O_2 \rightarrow Mn^{2+} + O_2^{-\bullet} + 2H^+$$
 (13)

$$Mn^{3+} + O_2^{-\bullet} \rightarrow Mn^{2+} + O_2$$
 (14)

$$Mn^{3+} + HO_{2} \rightarrow Mn^{2+} + O_2 + H^+$$
 (15)

$$Fe^{2+} + Mn^{3+} \leftrightarrow Fe^{3+} + Mn^{2+}$$
 (16)

$$PAHs + HO \bullet + O_2^{-\bullet} + O_2 \rightarrow byproducts + CO_2 + H_2O$$
 (17)

Therefore, the synergistic interactions between Fe^{2+}/Fe^{3+} and Mn^2+/Mn^{3+} redox couples at SBC active sites enhanced the catalytic activity. Moreover, the standard redox potential of Fe^{2+}/Fe^{3+} is 0.77 V vs. NHE and that of Mn^{2+}/Mn^{3+} is 1.51 V vs. NHE, which shows that electron transfer from Fe^{2+} to Mn^{3+} is thermodynamically spontaneous (Eqs. (18)–(20)) (Wen et al., 2019).

$$Fe^{3+} + e^{-} \rightarrow Fe^{2+}; E_{0} = 0.77 \text{ V vs. NHE}$$
 (18)

$$Mn^{3+} + e^{-} \rightarrow Mn^{2+}$$
; $E_{0} = 1.51 \text{ V vs. NHE}$ (19)

$$Fe^{2+} + Mn^{3+} \rightarrow Fe^{3+} + Mn^{2+}$$
; E = 0.74 V vs. NHE (20)

The activation of H₂O₂ by SBC produced HO[•] and redox Fe³⁺/ Fe²⁺ and Mn³⁺/Mn²⁺ pairs enabled efficient electron transfer, which together, accommodated the Haber-Weiss mechanism of AOPs (Danish et al., 2017). Further, reaction between HO• and H₂O produced H₂O₂, a strong oxidant and an essential Fenton reagent (Fig. 8a). PH, a typical LMW PAH with three fused benzene rings. was present at high levels in the PAH-contaminated sediment studied in the present research. In the absence of standard chemicals for the identification of intermediates, while based on information available in the literature (Bouzid et al., 2017; Yu et al., 2018; Chen et al., 2019), a conceptual reaction scheme was proposed for describing PH removal from contaminated marine sediments (Fig. 8b). The PH degradation pathway was suggested to described a series of reactions involved reactive radicals ($O_2^{-\bullet}$ and HO^{\bullet}) and benzene rings of parent compound and its intermediates. According to the pathway, $O_2^{-\bullet}$ and HO_{\bullet} , being generated from activated SPC, attacked the benzene ring of PH to trigger hydroxylation, decarboxylation, and cleavage of aromatic ring that formed a series of intermediates, including 9-phenanthrol, 9,10-phenanthrenediol, 9,10-phenanthrenequinone, 9,10-dihydroxyphenanthrene, anhydride, 2,2'-biphenyldicarboxylic acid, phthalic acid, 1,4hydroguinone, and 1,4-benzoguinone. Further attack of 9phenanthrol by the above radicals affords 9,10-phenanthrenediol, 9,10-phenanthrenequinone, 9,10-dihydroxyphenanthrene, and anhydride. Upon oxidation and ring opening, the anhydride is converted to 2,2'-biphenyldicarboxylic acid. Attack on 2,2'biphenyldicarboxylic acid by HO• yielded phthalic acid. Further oxidation of phthalic acid formed 1.4-hydroguinone and 1.4benzoquinone which were further mineralized to lactic acid, carbon dioxide, and water. Therefore, the byproducts produced during the SBC/SPC-mediated degradation of PAHs should be further

explored as to better assess the associated health and ecological risks.

4. Conclusion

The Fe- and Mn-rich water treatment plant sludge, a low-cost feedstock, was treated at different temperatures (300-900 °C) to produce sludge-derived biochar (SBC). SBC prepared at 700 °C exhibited the highest oxidative removal capacity of PAHs from contaminated aquatic sediments due to its higher activating SPC potential that led to the production of $HO \bullet$ and $O_2^{-\bullet}$ radical. PAHs containing 2-6 benzene rings were significantly removed over a wide pH range (pH 3.0-11.0) in the SBC matrix. The presence of crystalline Fe₃O₄ and Mn₃O₄ on the SBC surface enhanced PAHs oxidation via synergistic interactions between Fe²⁺/Fe³⁺ and Mn²⁺/ Mn³⁺ redox couples and active surface sites. Moreover, biochar effectively activated SPC and accelerated the formation of O₂[•] and HO• radicals for PAH degradation. Overall, results of this study not only presented a valuable management strategy on resource-based disposal of sludge, but also demonstrated that SBC/SPC system was highly effective in the removal of hazardous contaminants, such as PAH from contaminated sediments, further illustrating the benefits of environmental application of biosolids.

CRediT authorship contribution statement

Chang-Mao Hung: Conceptualization, Methodology, Investigation, Validation, Formal analysis, Writing - original draft. **Chin-Pao Huang:** Writing - review & editing, Visualization. **Chiu-Wen Chen:** Resources. **Chung-Hsin Wu:** Resources. **Yi-Li Lin:** Resources. **Cheng-Di Dong:** Resources, Supervision.

Fig. 8. (a) Proposed degradation mechanism of polycyclic aromatic hydrocarbon (PAH) over SBC catalyst and (b) reaction pathways of phenanthrene (PH) in the sulfate and hydroxyl radical-based advanced oxidation processes (Bouzid et al., 2017; Yu et al., 2018; Chen et al., 2019).

Declaration of competing interest

The authors declare that they have no known competing financial interests or personal relationships that could have appeared to influence the work reported in this paper.

Acknowledgments

The authors would like to thank the Ministry of Science and Technology of Taiwan, for financial support to perform this study under Contract Nos. MOST 106-2221-E-022-002-MY3, 106-2221-E-022-003-MY3 and 108-2221-E-992-051-MY3. The authors would like to thank Dr. Thanh-Binh Nguyen from National Kaohsiung University of Science and Technology for assistance of the EPR measurements. Addition support was provided by US NSF IOA (1632899) to CPH.

Appendix A. Supplementary data

Supplementary data to this article can be found online at https://doi.org/10.1016/j.envpol.2020.114914.

References

- Ahmad, M., Rajapaksha, A.U., Lim, J.E., Zhang, M., Bolan, N., Mohan, D., Vithanage, M., Lee, S.S., Ok, Y.S., 2014. Biochar as a sorbent for contaminant management in soil and water: a review. Chemosphere 99, 19–33.
- Baumard, P., Budzinski, H., Garrigues, P., Sorbe, J.C., Burgeot, T., Belloca, J., 1998. Concentration of PAH in various marine organisms in relation to those in sediments to trophic level. Mar. Pollut. Bull. 36, 951–960.
- Bouzid, I., Maire, J., Brunol, E., Caradec, S., Fatin-Rouge, N., 2017. Compatibility of surfactants with activated-persulfate for the selective oxidation of PAH in groundwater remediation. J. Environ. Chem. Eng. 5, 6098–6106.
- Chen, D., Yu, X., Song, C., Pang, X., Huang, J., Li, Y., 2016. Effect of pyrolysis temperature on the chemical oxidation stability of bamboo biochar. Bioresour. Technol. 218, 1303–1306.
- Chen, X., Yang, B., Oleszczuk, P., Gao, Y., Yuan, X., Ling, W., Waigi, M.G., 2019. Vanadium oxide activates persulfate for degradation of polycyclic aromatic hydrocarbons in aqueous system. Chem. Eng. J. 364, 79–88.
- Cui, H., Gu, X., Lu, S., Fu, X., Zhang, X., Fu, G.Y., Qiu, Z., Sui, Q., 2017. Degradation of ethylbenzene in aqueous solution by sodium percarbonate activated with EDDS–Fe(III) complex. Chem. Eng. J. 309, 80–88.
- Danish, M., Gu, X., Lu, S., Ahmad, A., Naqvi, M., Farooq, U., Zhang, X., Fu, X., Miao, Z., Xue, Y., 2017. Efficient transformation of trichloroethylene activated through sodium percarbonate using heterogeneous zeolite supported nano zero valent iron-copper bimetallic composite. Chem. Eng. J. 308, 396–407.
 De Luna, M.D.G., Sablas, M.M., Hung, C.M., Chen, C.W., Garcia-Segura, S., Dong, C.D.,
- De Luna, M.D.G., Sablas, M.M., Hung, C.M., Chen, C.W., Garcia-Segura, S., Dong, C.D., 2020. Modeling and optimization of imidacloprid degradation by catalytic percarbonate oxidation using artificial neural network and Box-Behnken experimental design. Chemosphere 251, 126254.
- Dong, C.D., Chen, C.W., Hung, C.M., 2017. Synthesis of magnetic biochar from bamboo biomass to activate persulfate for the removal of polycyclic aromatic hydrocarbons in marine sediments. Bioresour. Technol. 245, 188–195.
- Dong, C.D., Chen, C.W., Kao, C.M., Chien, C.C., Hung, C.M., 2018a. Wood-biocharsupported magnetite nanoparticles for remediation of PAH-contaminated estuary sediment. Catalysts 8, 73–86.
- Dong, C.D., Tsai, M.L., Chen, C.W., Hung, C.M., 2018b. Remediation and cytotoxicity study of polycyclic aromatic hydrocarbon-contaminated marine sediments using synthesized iron oxide—carbon composite. Environ. Sci. Pollut. Res. 6, 5243—5253.
- Dong, C.D., Chen, C.W., Tsai, M.L., Chang, J.H., Lyu, S.Y., Hung, C.M., 2019a. Degradation of 4-Nonylphenol in marine sediments by persulfate over magnetically modified biochars. Bioresour. Technol. 281, 143–148.
- Dong, C.D., Huang, C.P., Nguyen, T.B., Hsiung, C.F., Wu, C.H., Lin, Y.L., Chen, C.W., Hung, C.M., 2019b. The degradation of phthalate esters in marine sediments by persulfate over iron—cerium oxide catalyst. Sci. Total Environ. 696, 133973—133982.
- Dong, C.D., Lu, Y.C., Chang, J.H., Wang, T.H., Chen, C.W., Hung, C.M., 2019c. Enhanced persulfate degradation of PAH-contaminated sediments using magnetic carbon microspheres as the catalyst substrate. Process Saf. Environ. Protect. 125, 219–227
- Dong, C.D., Chen, C.W., Tsai, M.L., Hung, C.M., 2019d. The efficacy and cytotoxicity of iron oxide-carbon black composites for liquid-phase toluene oxidation by persulfate. Environ. Sci. Pollut. Res. 26, 14786–14796.
- Dong, C.D., Chen, C.W., Nguyen, T.B., Huang, C.P., Hung, C.M., 2020a. Degradation of phthalate esters in marine sediments by persulfate over Fe–Ce/biochar composites. Chem. Eng. J. 384, 123301.

- Dong, C.D., Tsai, M.L., Wang, T.H., Chang, J.H., Chen, C.W., Chen, C.W., 2020b. Removal of polycyclic aromatic hydrocarbon (PAH)-contaminated sediments by persulfate oxidation and determination of degradation product cytotoxicity based on HepG2 and ZF4 cell lines. Environ. Sci. Pollut. Res. https://doi.org/ 10.1007/s11356-019-04421-w.
- Du, J., Jing, C., 2018. Anthropogenic PAHs in lake sediments: a literature review (2002–2018). Environ. Sci. Proc. Impacts 20, 1649–1666.
- Fang, G., Gao, J., Liu, C., Dionysiou, D.D., Wang, Y., Zhou, D., 2014. Key role of persistent free radicals in hydrogen peroxide activation by biochar: implications to organic contaminant degradation. Environ. Sci. Technol. 48, 1902–1910.
- Fang, G., Liu, C., Gao, J., Dionysiou, D.D., Zhou, D., 2015. Manipulation of persistent free radicals in biochar to activate persulfate for contaminant degradation. Environ. Sci. Technol. 49, 5645–5653.
- Fu, X., Gu, X., Lu, S., Xu, M., Miao, Z., Zhang, X., Zhang, Y., Xue, Y., Qiu, Z., Sui, Q., 2016. Enhanced degradation of benzene in aqueous solution by sodium percarbonate activated with chelated-Fe(II). Chem. Eng. J. 285, 180—188.
- Fu, X., Gu, X., Lu, S., Sharma, V.K., Brusseau, M.L., Xue, Y., Danish, M., Fu, G.Y., Qiu, Z.,
 Sui, Q., 2017. Benzene oxidation by Fe(III)-activated percarbonate: matrix-constituent effects and degradation pathways. Chem. Eng. J. 309, 22–29.
 Guo, H., Kou, X., Zhao, Y., Wang, S., Sun, Q., Ma, X., 2018. Effect of synergistic
- Guo, H., Kou, X., Zhao, Y., Wang, S., Sun, Q., Ma, X., 2018. Effect of synergistic interaction between Ce and Mn on the CO₂ capture of calcium-based sorbent: textural properties, electron donation, and oxygen vacancy. Chem. Eng. J. 309, 22–29.
- Han, B., Zheng, L., Lin, F., 2019. Risk assessment and source apportionment of PAHs in surface sediments from Caofeidian Long Island, China. Mar. Pollut. Bull. 145, 42–46.
- Huang, Y.F., Huang, Y.Y., Chiueh, P.T., Lo, S.L., 2020. Heterogeneous Fenton oxidation of trichloroethylene catalyzed by sewage sludge biochar: experimental study and life cycle assessment. Chemosphere 249, 126139.
- Hung, C.M., Chen, C.W., Jhuang, Y.J., Dong, C.D., 2016a. Fe₃O₄ magnetic nanoparticles: characterization and performance exemplified by the degradation of methylene blue in the presence of persulfate. J. Adv. Oxid. Technol. 19, 43–51.
- Hung, C.M., Chen, C.W., Liu, Y.Y., Dong, C.D., 2016b. Decolorization of methylene blue by persulfate activated with FeO magnetic particles. Water Environ. Res. 88, 675–686.
- Hung, C.M., Huang, C.P., Hsieh, S.L., Tsai, M.L., Chen, C.W., Dong, C.D., 2020. Biochar derived from red algae for efficient remediation of 4-nonylphenol from marine sediments. Chemosphere 254, 126919.
- Jung, K.W., Choi, B.H., Jeong, T.U., Ahn, K.H., 2016. Facile synthesis of magnetic biochar/ Fe_3O_4 nanocomposites using electro-magnetization technique and its application on the removal of acid orange 7 from aqueous media. Bioresour. Technol. 220, 672–676.
- Kan, C.C., Chen, W.H., Wan, M.W., Phatai, P., Wittayakun, J., Li, K.F., 2012. The preliminary study of iron and manganese removal from groundwater by NaOCl oxidation and MF filtration. Sustain. Environ. Res. 22, 25–30.
- Kan, C.C., Sumalinog, M.J.R., Rivera, K.K.P., Arazo, R.O., de Luna, M.D.G., 2017. Ultrasound-assisted synthesis of adsorbents from groundwater treatment residuals for hexavalent chromium removal from aqueous solutions. Groundwater Sustain. Dev. 5, 253–260.
- Kottowski, M., Hilber, I., Bucheli, T.D., Charmas, B., Skubiszewska-Zieba, J., Oleszczuk, P., 2017. Activated biochars reduce the exposure of polycyclic aromatic hydrocarbons in industrially contaminated soils. Chem. Eng. J. 310, 33–40.
- Kumar, A., Sanger, A., Kumar, A., Kumar, Y., Chandra, R., 2016. An efficient α -MnO $_2$ nanorods forests electrode for electrochemical capacitors with neutral aqueous electrolytes. Electrochim. Acta 220, 712—720.
- Lemaire, J., Bués, M., Kabeche, T., Hanna, K., Simonnot, M.O., 2013. Oxidant selection to treat an aged PAH contaminated soil by in situ chemical oxidation. J. Environ. Chem. Eng. 1, 1261–1268.
- Li, C., Li, M., Bo, X., Yang, L., Mtukula, A.C., Guo, L., 2016. Facile synthesis of electrospinning Mn₂O₃-Fe₂O₃ loaded carbon fibers for electrocatalysis of hydrogen peroxide reduction and hydrazineoxidation. Electrochim. Acta 211, 255–264.
- Li, L., Lai, C., Huang, F., Cheng, M., Zeng, G., Huang, D., Li, B., Liu, S., Zhang, M., Qin, L., Li, M., He, J., Zhang, Y., Chen, L., 2019a. Degradation of naphthalene with magnetic bio-char activate hydrogen peroxide: synergism of bio-char and FeMn binary oxides. Water Res. 160, 238–248.
- Li, L., Huang, J., Hu, X., Zhang, S., Dai, Q., Chai, H., Gu, L., 2019b. Activation of sodium percarbonate by vanadium for the degradation of aniline in water: mechanism and identification of reactive species. Chemosphere 215, 647–656.
- Lin, K.Y.A., Lin, J.T., Lin, Y.F., 2017. Heterogeneous catalytic activation of percarbonate by ferrocene for degradation of toxic amaranth dye in water. J. Taiwan Inst. Chem. Eng. 78, 144–149.
- Liu, Q., Fang, Z., Liu, Y., Liu, Y., Xu, Y., Ruan, X., Zhang, X., Cao, W., 2019. Phosphorus speciation and bioavailability of sewage sludge derived biochar amended with CaO. Waste Manag. 87, 71–77.
- Maletić, S.P., Beljin, J.M., Rončević, S.D., Grgić, M.G., Dalmacija, B.D., 2019. State of the art and future challenges for polycyclic aromatic hydrocarbons is sediments: sources, fate, bioavailability and remediation techniques. J. Hazard Mater. 365, 467–482.
- Meng, Y., Liu, X., Lu, S., Zhang, T., Jin, B., Wang, Q., Tang, Z., Liu, Y., Guo, X., Zhou, J., Xi, B., 2019. A review on occurrence and risk of polycyclic aromatic hydrocarbons (PAHs) in lakes of China. Sci. Total Environ. 651, 2497–2506.
- Mian, M.M., Liu, G., 2018. Recent progress in biochar-supported photocatalysts: synthesis, role of biochar, and applications. RSC Adv. 8, 14237.
- Miao, Z., Gu, X., Lu, S., Brusseau, M.L., Zhang, X., Fu, X., Danish, M., Qiu, Z., Sui, Q.,

- 2015. Enhancement effects of chelating agents on the degradation of tetra-chloroethene in Fe(III) catalyzed percarbonate system. Chem. Eng. J. 281, 286–204
- Mohamed, I., Zhang, G., Li, Z., Liu, Y., Chen, F., Dai, K., 2015. Ecological restoration of an acidic Cd contaminated soil using bamboo biochar application. Ecol. Eng. 84, 67–76.
- Mojiri, A., Zhou, J.L., Ohashi, A., Ozaki, N., Kindaichi, T., 2019. Comprehensive review of polycyclic aromatic hydrocarbons in water sources, their effects and treatments. Sci. Total Environ. 696, 133971.
- Ruan, X., Sun, Y., Du, W., Tang, Y., Liu, Q., Zhang, Z., Doherty, W., Frost, R.L., Qian, G., Tsang, D.C.W., 2019. Formation, characteristics, and applications of environmentally persistent free radicals in biochars: a review. Bioresour. Technol. 281, 457–468.
- Tao, S., Yang, J., Hou, H., Liang, S., Xiao, K., Qiu, J., Hu, J., Liu, B., Yu, W., Deng, H., 2019. Enhanced sludge dewatering via homogeneous and heterogeneous Fenton reactions initiated by Fe-rich biochar derived from sludge. Chem. Eng. J. 372, 966–977.
- Wang, J., Shen, M., Gong, Q., Wang, X., Cai, J., Wang, S., Chen, Z., 2020. One-step preparation of ZVI-sludge derived biochar without external source of iron and its application on persulfate activation. Sci. Total Environ. 714, 136728.
- Wang, R.Z., Huang, D.L., Liu, Y.G., Zhang, C., Lai, C., Wang, X., Zeng, G.M., Gong, X.M., Duan, A., Zhang, Q., Xu, P., 2019a. Recent advances in biochar-based catalysts: properties, applications and mechanisms for pollution remediation. Chem. Eng. J. 371, 380–403.
- Wang, X., Chi, Q., Liu, X., Wang, Y., 2019b. Influence of pyrolysis temperature on characteristics and environmental risk of heavy metals in pyrolyzed biochar

- made from hydrothermally treated sewage sludge. Chemosphere 216, 698–706. Wen, Z., Lu, J., Zhang, Y., Cheng, G., Guo, S., Wei, P., Ming, Y., Wang, Y., Chen, R., 2019. Simultaneous oxidation and immobilization of arsenite from water by nanosized magnetic mesoporous iron manganese bimetal oxides (NanosizedMMIM): synergistic effect and interface catalysis. Chem. Eng. J. (in press).
- Xia, H., Zhang, Z., Liu, J., Deng, Y., Zhang, D., Du, P., Zhang, S., Lu, X., 2019. Novel Fe-Mn-O nanosheets/wood carbon hybrid with tunable surface properties as a superior catalyst for Fenton-like oxidation. Appl. Catal. B Environ. 259, 118058—118069.
- Xu, T., Lou, L., Luo, L., Cao, R., Duan, D., Chen, Y., 2012. Effect of bamboo biochar on pentachlorophenol leachability and bioavailability in agricultural soil. Sci. Total Environ. 414, 727–731.
- Yu, S., Gu, X., Lu, S., Xue, Y., Zhang, X., Xu, M., Qiu, Z., Sui, Q., 2018. Degradation of phenanthrene in aqueous solution by a persulfate/percarbonate system activated with CA chelated-Fe(II). Chem. Eng. J. 333, 122—131.
- Zhang, J., Lü, F., Zhang, H., Shao, L., Chen, D., He, P., 2015. Multiscale visualization of the structural and characteristic changes of sewage sludge biochar oriented towards potential agronomic and environmental implication. Sci. Rep. 5, 9406.
- Zhang, L., Nie, Y., Hu, C., Hu, X., 2011. Decolorization of methylene blue in layered manganese oxide suspension with $\rm H_2O_2$. J. Hazard Mater. 190, 780–785.
- Zhao, D., Liao, X., Yan, X., Huling, S.G., Chai, T., Tao, H., 2013. Effect and mechanism of persulfate activated by different methods for PAHs removal in soil. J. Hazard Mater. 254–255, 228–235.
- Zheng, Z.J., Lin, M.Y., Chiueh, P.T., Lo, S.L., 2019. Framework for determining optimal strategy for sustainable remediation of contaminated sediment: a case study in Northern Taiwan. Sci. Total Environ. 654. 822—831.